Competition between structural distortion and magnetic moment formation in fullerene C_{20}

Myung Joon Han,[1] Gunn Kim,[2] Jae Il Lee,[3] and Jaejun Yu[4,a)]
[1]*Department of Physics, University of California, Davis, One Shields Avenue, Davis, California 95616, USA*
[2]*Department of Physics and Astronomy and FPRD, Seoul National University, Seoul 151-747, Korea*
[3]*Department of Physics, Inha University, Incheon 402-751, Korea*
[4]*Department of Physics and Astronomy, CSCMR, Seoul National University, Seoul 151-747, Korea*

(Received 20 September 2008; accepted 23 March 2009; published online 12 May 2009)

We investigate the effect of on-site Coulomb interactions on the structural and magnetic ground state of C_{20} fullerene based on density-functional-theory calculations within the local density approximation (LDA) plus on-site Coulomb corrections (LDA+U). The total energies of the high symmetry (I_h) and the distorted (D_{3d}) structures of C_{20} are calculated for different spin configurations. The ground state configurations are found to depend on the forms of exchange-correlation potentials and the on-site Coulomb interaction parameter U, reflecting the subtle nature of the competition between Jahn–Teller distortion and magnetic instability in the C_{20} fullerene. While the nonmagnetic state of the distorted D_{3d} structure is robust for small U, a magnetic ground state of the undistorted I_h structure emerges for U larger than 4 eV when the LDA exchange-correlation potential is employed. © *2009 American Institute of Physics*.
[DOI: 10.1063/1.3119485]

I. INTRODUCTION

Since the discovery of fullerene C_{60} (Ref. 1) various research activities on alternative fullerene structures of carbon materials have flourished due to their noble physical properties and potential applications as next generation electronic devices. The smallest fullerene C_{20} has been actively studied after its first successful production by Prinzbach *et al.*[2] Although there have been many theoretical predictions on its intriguing properties such as superconductivity,[3] vibrational modes,[4,5] and transport[6–8] along the line of fullerene-based molecular electronics,[9,10] C_{20} has been a challenge for theorists since long before its experimental synthesis. For instance, the stable structural configuration of C_{20} has not been clearly understood. The effort to determine the stable structure and relative stability of C_{20} isomers, e.g., ring, bowl, and cage, has raised a question on the contribution of electron correlation energy to the structural stability.[11–14] One of the difficulties in predicting the most stable C_{20} isomer lies in the treatment of exchange-correlation (XC) energy. It was shown that density-functional-theory (DFT) calculations gave qualitatively different results depending on the XC functional such as local density approximation (LDA), generalized gradient approximation (GGA), and Hartree–Fock (HF). Even quantum Monte Carlo (QMC) results were different from LDA, GGA, HF, and hybrid DFT.[13]

The prediction of the ground state atomic structure of the C_{20} fullerene has suffered a similar problem. The high symmetry I_h structure of the C_{20} cage is known to be unstable with respect to the Jahn-Teller (JT) distortion. According to Galli *et al.*,[14] both LDA and GGA predicted D_{3d} as the symmetry of the most stable JT distorted cage structure, which is consistent with the tight-binding molecular-dynamics result by Yamamoto *et al.*[8] However, the hybrid DFT calculation by Saito and Miyamoto[4] determined C_{2h} to be the most stable one, while C_2 or D_{5d} were chosen by the HF calculations.[14] Sometimes even the same kind of calculations made by different groups has given different predictions (see, for example, Ref. 14). As Grossman *et al.*[13] pointed out, this small molecular carbon system, C_{20}, demonstrates the importance of the highly accurate treatment of electron correlations.

Recently Lin *et al.*[15,16] took a different perspective to this issue. By considering the fullerene C_{20} as a superatom with 20 valence electrons, they set up a tight-binding model taking account of the strong hybridization of p_π-orbitals with p_σ, which arises from the extreme curvature of the C_{20} cage. Expecting the important role of the on-site Coulomb interaction, they carried out QMC and exact diagonalization (ED) calculations for the Hubbard model Hamiltonian for C_{20}. As a result, they found that C_{20} with both I_h and D_{3d} structures undergoes a magnetic-to-nonmagnetic (NM) and NM-to-magnetic transitions for I_h and D_{3d}, respectively, as U/t increases.[15,16]

To investigate the effect of the on-site Coulomb interaction in connection with the atomic and magnetic structures of its ground state, we performed the LDA+U and GGA+U calculations[17] and calculated optimized structure under the symmetry constraint of I_h and D_{3d}. Our result showed that the NM D_{3d} structure is more stable than magnetic I_h for small values of U less than 4 eV regardless of the choice of the XC functionals, which is consistent with previous works.[8,14] However, when $U>4$ eV, the LDA+U calculations predict a magnetic state with $\mu=2\mu_B$ to be a ground state, which is different from GGA+U. This result indicates

a)Author to whom correspondence should be addressed. Electronic mail: jyu@snu.ac.kr.

that there are subtleties in the competition between the JT structural instability and the magnetic instability enhanced by Coulomb correlations. Further the dependence on the XC functionals suggests the importance of electron correlation effects in determination of the C_{20} ground state.

II. COMPUTATIONAL METHODS

A. LDA+*U* method

In order to describe the on-site Coulomb interactions for the carbon $2p$ orbitals, which are relatively localized in a small-sized cluster such as C_{20}, we employed the LDA+U (GGA+U) method.[17,18] In our LDA+U (GGA+U) approach, the total energy functional is written as[18]

$$E_{\mathrm{LDA}+U(\mathrm{GGA}+U)} = E_{\mathrm{LDA(GGA)}} + E_U^0 - E_{\mathrm{dc}}^U, \tag{1}$$

where $E_{\mathrm{LDA(GGA)}}$ is the LDA (GGA) energy functional and E_U^0 is given by a spherically averaged screened-Coulomb energy U and an exchange energy J,

$$E_U^0 = \frac{1}{2}\sum_{\alpha} U_\alpha \sum_{\sigma m m'} n_{\alpha m}^{\sigma} n_{\alpha m'}^{-\sigma} + \frac{1}{2}\sum_{\alpha} (U_\alpha - J_\alpha) \sum_{\sigma, m \neq m'} n_{\alpha m}^{\sigma} n_{\alpha m'}^{\sigma}, \tag{2}$$

where σ is the spin index and $\alpha \equiv (ilp)$, with the site index i, the angular momentum quantum number l, and the multiplicity number of the radial basis function $pn_{\alpha m}^{\sigma}$ is an eigenvalue of the occupation number matrix. Here the U- and the J-values are assumed to depend only on the index α but to be independent of the azimuthal quantum number m, which is regarded as a simplification of the HF theory by using a spherical average. The double-counting term E_{dc}^U can be written as

$$E_{\mathrm{dc}}^U = \frac{1}{2}\sum_{\alpha} U_\alpha N_\alpha (N_\alpha - 1) - \frac{1}{2}\sum_{\alpha} J_\alpha \sum_{\sigma} N_\alpha^{\sigma}(N_\alpha^{\sigma} - 1), \tag{3}$$

where $N_\alpha^{\sigma} = \Sigma_m n_{\alpha m}^{\sigma}$ and $N_\alpha = N_\alpha^{\uparrow} + N_\alpha^{\downarrow}$. Therefore, $E_U \equiv E_U^0 - E_{\mathrm{dc}}^U$ reads

$$E_U = \frac{1}{2}\sum_{\alpha} (U_\alpha - J_\alpha) \sum_{\sigma} \{\mathrm{Tr}(n_\alpha^{\sigma}) - \mathrm{Tr}(n_\alpha^{\sigma} n_\alpha^{\sigma})\}, \tag{4}$$

and it is the term that describes the on-site Coulomb interactions. The effective U-value, defined by $U = U_\alpha - J_\alpha$, can be treated as a numerical parameter, and it is clear from Eq. (4) that LDA+U (GGA+U) method is equivalent to LDA (GGA) in $U \to 0$ limit. We used the previously proposed "dual" representation,[18] which is proven to be successful for various materials.[19–21]

B. Computation details

We performed cluster calculations based on the DFT by employing a linear-combination-of-localized-pseudoatomic orbitals as a basis set. Ceperley–Alder[22,23] and Perdew–Burke–Ernzerhof[24] type XC energy functionals were adopted for LDA and GGA calculations, respectively. We used double valence orbitals as a basis set, which were generated by a confinement potential scheme with the cutoff radius of 5.0 a.u. Troullier–Martins-type pseudopotentials with a partial core correction were used to replace deep core potentials by the norm-conserving soft potentials in a factorized separable form with multiple projectors. Real space grid techniques were used with the energy cutoff of 160 Ry in numerical integrations and the solution of the Poisson equation using fast Fourier transformations. In addition, the projector expansion method was employed to accurately calculate three-center integrals associated with the deep neutral atom potential with $L_{\max}=6$ and $N_{\mathrm{rad}}=4$. All the DFT calculations were performed using our DFT OPENMX code.[25]

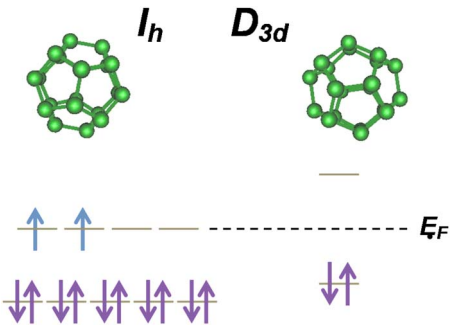

FIG. 1. (Color online) Hückel's molecular orbital levels for the highly symmetric I_h structure and the JT distorted D_{3d} structure of C_{20}. Up and down arrows indicate up and down spin electrons, respectively. The horizontal dashed line represents the Fermi level.

III. RESULT AND DISCUSSION

Figure 1 shows a schematic diagram of the Hückel's molecular orbital levels around the Fermi energy for the magnetic I_h and the JT distorted D_{3d} structure of C_{20} fullerene. In the highly symmetric I_h structure, the highest-occupied-molecular-orbital (HOMO) states are fourfold degenerate and partially filled by two valence electrons. Due to the electronic degeneracy, the I_hC_{20} is JT active and can undergo a structural distortion. Consequently the JT distorted D_{3d} structure leads to a finite gap in between the HOMO level and the lowest-unoccupied-molecular-orbital (LUMO) states. Since the HOMO state is occupied by a singlet pair, the D_{3d} ground state becomes NM. On the other hand, the I_hC_{20} ground state can be magnetic due to a kind of the Hund's rule coupling present in this "superatom," where the magnetic exchange energy between the HOMO electrons favors the ferromagnetic (FM) spin configuration of the undistorted I_h structure.

The calculated density-of-states (DOS) in Fig. 2 clearly shows the different electronic structures of these two structures. The dotted and solid lines correspond to the $U=0$ and $U=2$ eV calculations, respectively. The Fermi level of I_hC_{20} is located at the middle of a majority spin peak [Fig. 2(a)], whereas D_{3d} has a finite HOMO-LUMO gap [Fig. 2(b)], which is consistent with the Hückel's molecular orbital pictures in Fig. 1. While the electronic states of the JT distorted D_{3d} structure are hardly affected by the change of on-site U values from 0 to 2 eV, the exchange split of the undistorted I_h structure is significantly enhanced even for the moderate on-site interaction of $U=2$ eV. Considering the enhanced ex-

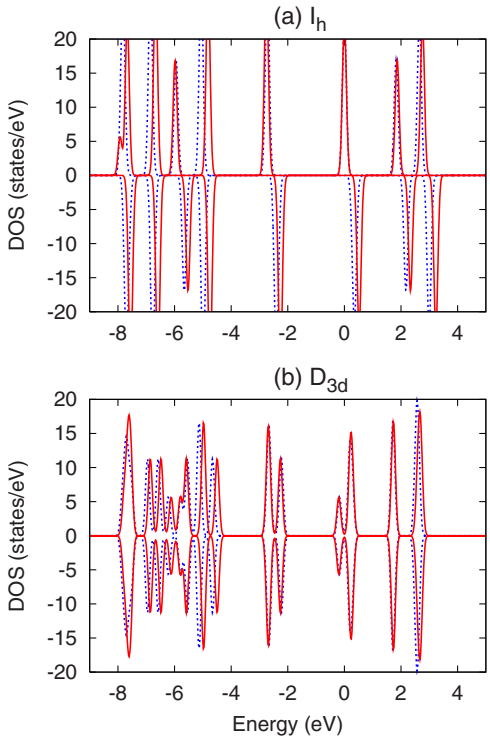

FIG. 2. (Color online) Total DOS for (a) I_h and (b) D_{3d} structure C_{20} fullerene. Up and down panels refer to the up-spin and down-spin states, and the dotted and solid lines correspond to $U=0$ and 2 eV, respectively. The DOS plots were drawn with the Gaussian broadening of 0.1 eV, and the Fermi energy is set at zero.

change interactions, we tried to explore a possible contribution of the on-site Coulomb interactions to the stabilization of the magnetic I_h structure over that of the JT structural distortion.

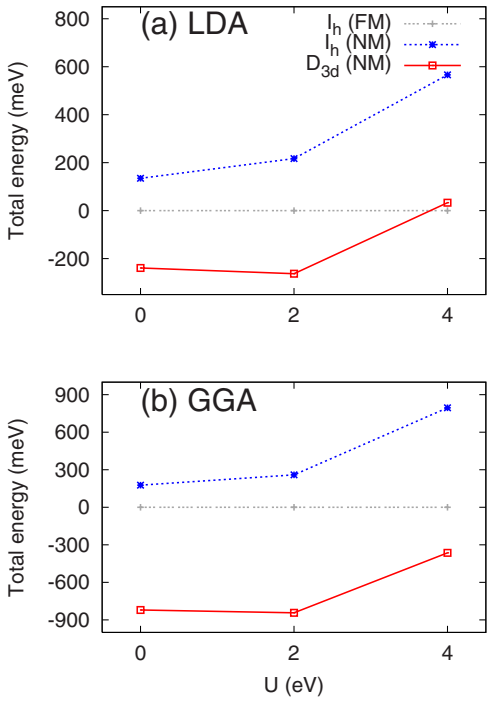

FIG. 3. (Color online) Total energy curves as a function of U. The calculated energies of NM-I_h (dotted line with $*$-mark) and NM-D_{3d} (solid line with □-mark) are plotted with respect to that of FM-I_h (dotted line with +-mark) in meV unit.

TABLE I. LDA+U and GGA+U total energies (in meV unit) of the I_h and D_{3d} structures of C_{20} with FM and NM spin configurations as a function of U. FM-D_{3d} converges to be NM spin state in $U=0$, 2 eV (see the text). The total energies are given relative to that of FM-I_h.

XC-type	Symmetry	$U=0$ eV	$U=2$ eV	$U=4$ eV
LDA	I_h (FM)	0	0	0
	I_h (NM)	135	217	566
	D_{3d} (NM)	−239	−263	33
GGA	I_h (FM)	0	0	0
	I_h (NM)	177	259	795
	D_{3d} (NM)	−821	−843	−364

Figure 3 shows the calculated total energies by LDA+U [Fig. 3(a)] and GGA+U [Fig. 3(b)] as a function of U. For comparison, we also calculated the total energies of the NM phase of I_h. The total energies of FM-I_h, NM-I_h, and NM-D_{3d} are represented by the dotted (with+-mark), dotted (with $*$-mark), and solid (with □-mark) lines, respectively. The total energy of FM-I_h is set at zero as a reference. For the both LDA and GGA calculations with $U=0$, the NM-D_{3d} configuration was found to be the ground state, and the NM-I_h configuration is the highest in energy, which is consistent with the JT structural instability of I_h discussed above. GGA predicts the larger stability of the NM-D_{3d} over the magnetic FM-I_h. The stabilization energy of the NM-D_{3d} over FM-I_h and NM-I_h is 239 and 374 meV, in LDA, whereas 821 and 998 meV in GGA, respectively. (See Table I for detailed information.) The relative order of stability among the different configurations remains the same even with $U=2$ eV.

It is noted that the D_{3d} structure is stabilized over I_h in GGA calculation than in LDA for both $U=0$ and 2 eV; the stabilization energy is more than three times larger than in LDA. With a larger Coulomb interaction parameter, $U=4$ eV, The total energy differences between FM-I_h and NM-D_{3d} are dramatically reduced for both LDA+U and GGA+U results. Indeed, in the case of LDA+U, the ground state is changed from the NM-D_{3d} to the FM-I_h configuration

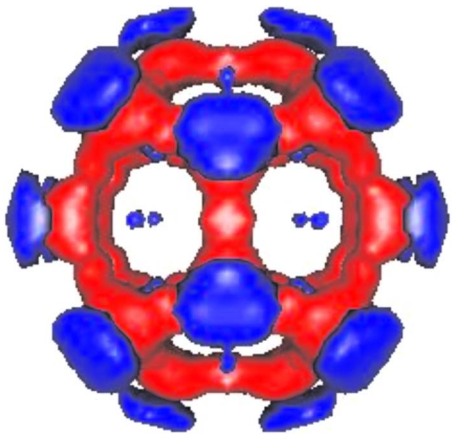

FIG. 4. (Color online) Isosurface plot of the charge density difference of FM I_h between $U=0$ eV and $U=2$ eV. Dark-gray and light-gray surfaces correspond to electron surplus regions for $U=2$ eV and $U=0$ eV, respectively, at the isovalue of 0.7×10^{-3} e Å^{-3}.

as shown in Fig. 3. This result implies that when U becomes large, the magnetic energy gain with an enhanced exchange interaction can stabilize the symmetric I_h structure against the JT distortion with a lower symmetry D_{3d} structure. The strong on-site Coulomb interactions enhance the electron localization, which leads to the exchange energy gain, thereby contributing to the stabilization of the undistorted structure. Figure 4 shows a charge density difference between $U=2$ and $U=0$ of FM-I_h. The dark-gray and light-gray colors represent the electron surplus regions of the $U=2$ and $U=0$ eV calculations, respectively. Though the magnitude of the charge difference is small, the difference plot in Fig. 4 demonstrates the tendency of electron localization at each carbon site, which arises from the electron correlation due to the on-site Coulomb interactions. The effect of the electron localization can affect a relatively enhanced exchange coupling among the degenerate HOMO states, and its magnitude seems to be comparable to that of the JT distortion. Figure 2 shows that the JT level spacing in Fig. 2(b) is comparable to that of the exchange splitting in Fig. 2(a). Since the JT distortion lifts up the orbital degeneracy of the HOMO states, the JT mechanism acts against the formation of magnetic moment in fullerene C_{20}. This result is another example demonstrating the discrepancy caused by the different XC energy functionals and further is consistent with the previous studies,[13,14] which emphasized that the structural ground state depend on the type of XC energy functionals.

It is interesting to compare our LDA+U and GGA+U calculation results with a recent Hubbard-model-based study by Lin *et al.*[15] Starting from an observation that the hopping parameter t of the C_{20} fullerene should be much smaller than that of C_{60}, but its on-site repulsion U remains the same, which means that the ratio of U/t is large, they assumed that electron correlations play an important role in this system and performed ED and QMC calculation for one-band Hubbard model parametrized by U/t,

$$H = -t \sum_{\langle i,j\rangle,\sigma} (c_{i\sigma}^{\dagger} c_{j\sigma} + Hc) + U \sum_{i} n_{i\uparrow} n_{i\downarrow}. \quad (5)$$

Their results predicted that the ground state of the I_h structure changes from triplet to singlet at about $U/t \approx 4.10$, while the ground state of D_{3d} evolves from the singlet (NM) state at $U=0$ to a triplet state for U/t larger than 0.5 and then transit to a singlet state again at $U/t \approx 4.19$. Those predictions based on the model analysis are in contradiction to our DFT calculations, where the FM state of the I_h structure is always stable relative to the NM I_h state and the JT distorted D_{3d} structure prefers a NM ground state. The main difference between the Hubbard model approach and our DFT calculations lies on that our DFT calculations take account of the exchange coupling among the electrons occupying the HOMO states. The explicit treatment of the degenerate HOMO states is crucial since the energetic competition between the exchange coupling and the JT structural distortion is crucial for the degenerate states.

IV. CONCLUSION

We investigated the effect of on-site Coulomb correlations on the structural and magnetic properties of the fullerene C_{20} by carrying out the LDA+U and GGA+U calculations. From the comparison of the total energies of the magnetic I_h structure and the JT distorted D_{3d} structure for different values of the on-site Coulomb interaction U, we suggest that the magnetic instability by the Coulomb correlation can possibly override the JT structural distortion at least for the value of $U=4$ eV within the LDA+U calculations. Considering the subtle dependence of the ground state properties of C_{20} on the choice of XC-functional forms as well as the Hubbard model parameters, more elaborate calculations are required to resolve the physical picture for the ground state of the fullerene C_{20}, where the magnetic instability due to the Coulomb correlation effect competes with the structural distortion in the superatom fullerene C_{20}.

ACKNOWLEDGMENTS

This work was supported by the KOSEF through the ARP (Grant No. R17-2008-033-01000-0). G.K. acknowledges the support by the post-BK project. The calculations were carried out at the KISTI Supercomputing Center under the Supercomputing Application Support Program.

[1] H. W. Kroto, J. R. Heath, S. C. O'Brien, R. F. Curl, and R. E. Smalley, Nature (London) **318**, 162 (1985).
[2] H. Prinzbach, A. Weiler, P. Landenberger, F. Wahl, J. Wörth, L. T. Scott, M. Gelmont, D. Olevano, and B. Issendorff, Nature (London) **407**, 60 (2000).
[3] Y. Miyamoto and M. Saito, Phys. Rev. B **63**, 161401(R) (2001).
[4] M. Saito and Y. Miyamoto, Phys. Rev. Lett. **87**, 035503 (2001).
[5] M. Saito and Y. Miyamoto, Phys. Rev. B **65**, 165434 (2002).
[6] C. Roland, B. Larade, J. Taylor, and H. Guo, Phys. Rev. B **65**, 041401(R) (2001).
[7] M. Otani, T. Ono, and K. Hirose, Phys. Rev. B **69**, 121408(R) (2004).
[8] T. Yamamoto, K. Watanabe, and S. Watanabe, Phys. Rev. Lett. **95**, 065501 (2005).
[9] H. Park, J. Park, A. K. L. Lim, E. H. Anderson, A. P. Alivisatos, and P. L. McEuen, Nature (London) **407**, 57 (2000).
[10] A. N. Pasupathy, J. Park, C. Chang, A. V. Soldatov, S. Lebedkin, R. C. Bialczak, J. E. Grose, L. A. K. Donev, J. P. Sethna, D. C. Ralph, and P. L. McEuen, Nano Lett. **5**, 203 (2005).
[11] V. Parasuk and J. Almlöf, Chem. Phys. Lett. **184**, 187 (1991).
[12] B. L. Zhang, C. Z. Wang, K. M. Ho, C. H. Xu, and C. T. Chan, J. Chem. Phys. **97**, 5007 (1992).
[13] J. C. Grossman, L. Mitas, and K. Raghavachari, Phys. Rev. Lett. **75**, 3870 (1995).
[14] G. Galli, F. Gygi, and J.-C. Golaz, Phys. Rev. B **57**, 1860 (1998).
[15] F. Lin, E. S. Sørensen, C. Kallin, and A. J. Berlinsky, Phys. Rev. B **76**, 033414 (2007).
[16] F. Lin, E. S. Sørensen, C. Kallin, and A. J. Berlinsky, J. Phys.: Condens. Matter **19**, 456206 (2007).
[17] V. I. Anisimov, F. Aryasetiawan, and A. I. Lichtenstein, J. Phys.: Condens. Matter **9**, 767 (1997).
[18] M. J. Han, T. Ozaki, and J. Yu, Phys. Rev. B **73**, 045110 (2006).
[19] M. J. Han and J. Yu, J. Korean Phys. Soc. **48**, 1496 (2006).
[20] K. An, N. Lee, J. Park, S. C. Kim, Y. Hwang, J.-G. Park, J.-Y. Kim, J.-H. Park, M. J. Han, J. Yu, and T. Hyeon, J. Am. Chem. Soc. **128**, 9753 (2006).
[21] M. J. Han, T. Ozaki, and J. Yu, Phys. Rev. B **75**, 060404 (2007).
[22] D. M. Ceperley and B. J. Alder, Phys. Rev. Lett. **45**, 566 (1980).
[23] J. P. Perdew and A. Zunger, Phys. Rev. B **23**, 5048 (1981).
[24] J. P. Perdew, K. Burke, and M. Ernzerhof, Phys. Rev. Lett. **77**, 3865 (1996).
[25] The OPENMX DFT code used in this study is available on a web site (http://www.openmx-square.org/) in the constitution of the GNU General Public License.